Flux-tube structure and β functions in SU(2)

P. Pennanen* and A. M. Green†
Helsinki Institute of Physics, University of Helsinki, Helsinki, Finland

C. Michael‡
Theoretical Physics Division, Department of Mathematical Sciences, University of Liverpool, Liverpool, United Kingdom

(Received 23 May 1997)

The spatial distribution of the action and energy in the color fields of flux tubes is studied in lattice SU(2) field theory for static quarks at separations up to 1 fm at $\beta=2.4,2.5$. The ground and excited states of the color fields are considered. Sum rules are used to get estimates of generalized β functions. [S0556-2821(97)06619-8]

PACS number(s): 11.15.Ha, 12.38.Gc, 13.75.−n, 24.85.+p

I. INTRODUCTION

Nonperturbative phenomena of QCD such as confinement can be explored using Monte Carlo simulations of lattice gauge theory. The potential $V(R)$ between two static quarks at separation R in quenched QCD is one of the simplest manifestations of confinement and has been studied intensively. At large R the potential rises linearly as predicted by the hadronic string model. One can also measure the spatial distribution of the color fields around such static quarks in order to get a detailed picture of the confining flux tube. In Ref. [1], which contains references to earlier work, this was done for the ground state and the first excited state of the two-quark potential, having the symmetries of the A_{1g} and E_u representations, respectively, of the lattice symmetry group D_{4h}. Transverse and longitudinal profiles of chromoelectric and -magnetic fields were compared with vibrating string and dual QCD models for the flux tube, with the latter model reproducing quite well the shape of the energy profile measured on a lattice. Instead of SU(3), the gauge group used was SU(2), which is more manageable with present-day computer resources and is expected to have very similar features of confinement. This is reflected in the fact that the flux-tube models considered do not distinguish between SU(2) and SU(3).

The method used to study the color fields on a lattice is to measure the correlation of a plaquette $\square\equiv\frac{1}{2}\,\mathrm{Tr}(1-U_{\square})$ with the Wilson loop $W(R,T)$ that represents the static quark and antiquark at separation R. When the plaquette is located at $t=T/2$ in the μ-ν plane, the following expression isolates, in the limit $T\to\infty$, the contribution of the color field at position $\mathbf{r}$:

$$f_R^{\mu\nu}(\mathbf{r})=\left[\frac{\langle W(R,T)\square_{\mathbf{r}}^{\mu\nu}\rangle-\langle W(R,T)\rangle\langle\square^{\mu\nu}\rangle}{\langle W(R,T)\rangle}\right]. \quad (1.1)$$

In the naive continuum limit these contributions are related to the mean squared fluctuation of the Minkowski color fields by

$$f_R^{ij}(\mathbf{r})\to\frac{a^4}{\beta}\,B_k^2(\mathbf{r}) \quad \text{with } i,j,k \text{ cyclic},$$

$$f_R^{i4}(\mathbf{r})\to-\frac{a^4}{\beta}E_i^2(\mathbf{r}). \quad (1.2)$$

When the interquark separation axis is chosen as the 1 axis the squares of the longitudinal and transverse electric and magnetic fields can be identified as

$$\mathcal{E}_L=f^{41},\quad \mathcal{E}_T=f^{42,43},\quad \mathcal{B}_T=f^{12,13},\quad \mathcal{B}_L=f^{23,32}. \quad (1.3)$$

These can then be combined naively to give the action density

$$S(\mathbf{r})=-(\mathcal{E}_L+2\mathcal{E}_T+2\mathcal{B}_T+\mathcal{B}_L) \quad (1.4)$$

and the energy density

$$E(\mathbf{r})=E_L(\mathbf{r})+2E_T(\mathbf{r})=-(\mathcal{E}_L-\mathcal{B}_L)-2(\mathcal{E}_T-\mathcal{B}_T) \quad (1.5)$$

of the gluon field.

Since in this work we use a plaquette to probe the color flux, the spatial size of the probe will decrease as the lattice spacing $a\to0$. To define a continuum limit of the color flux distributions, one would have to use a probe of a fixed physical size as $a\to0$. In this work we wish to compare flux distributions at different lattice spacing. One special tool that is available, when a plaquette is used to probe the color flux with the Wilson gauge action, is that exact identities can be derived for the integrals over all space of the flux distributions. These sum rules [2–5] relate spatial sums of the color fields measured using Eq. (1.1) to the static potential $V(R)$ via generalized β functions, which show how the bare couplings of the theory vary with the generalized lattice spacings a_μ in four directions. One can think of these sum rules as providing the appropriate anomalous dimension for the color flux sums. This normalizes the color flux and provides a guide for comparing color flux distributions measured at dif-

*Electronic address: petrus.pennanen@helsinki.fi
†Also at Department of Physics, University of Helsinki, Helsinki, Finland. Electronic address: green@phcu.helsinki.fi
‡Electronic address: cmi@liv.ac.uk

ferent a values. The full set of sum rules [5] allows these generalized β functions to be determined at just one β value (see [6] and references therein). Here we investigate this further by comparing estimates at two different β values. This can also help to clear up some inconsistencies between the β-function determination from the sum rules at one β value [6] and other methods [7,8].

In Ref. [1] the simulations were carried out at $\beta=2.4$ with a $16^3\times 32$ lattice. Here results from similar computations at $\beta=2.5$ with a $24^3\times 32$ lattice are reported. Most of the simulation and analysis techniques, such as use of a variational basis with different fuzzing levels, are the same and can be found from Ref. [1]. In addition to more accurate measurements of flux-tube profiles, we also present estimates of β functions at both $\beta=2.4$ and 2.5.

In Sec. II static quark-quark potentials $V(R)$ are extracted and in Sec. III the corresponding flux tube profiles are calculated. In Sec. IV, $V(R)$ and the profiles are related by sum rules and various estimates of the β function are made. Some conclusions are made in Sec. V.

II. STATIC POTENTIALS

Accurate estimates of the potential energy between two static quarks are needed for the extraction of β functions to be presented in Sec. IV. In addition to small statistical errors, ''accurate'' means that the gluonic state measured has little contamination from other states. This is achieved by diagonalizing a variational basis of different paths connecting the same points on the lattice. Below we present estimates of the remaining contamination in our observables. The fundamental question concerning the scale, i.e., the value of the lattice spacing a in physical units, is also answered using the two-body potentials.

We construct lattice operators to create and destroy states with two static quarks at separation R joined by gluonic paths that represent the color flux. The techniques we use to make efficient operators with a large overlap with the ground state are described in detail in Ref. [1]. In order to improve the signal we applied ''fuzzing,'' where each spatial link is replaced by a weighted sum of itself and its surrounding spatial staples, before the correlations were measured. To investigate gluonic excitations and minimize their contribution to the ground-state signal we need a variational basis, which was obtained by performing the measurements on lattices with different levels of fuzzing.

At $\beta=2.4$,2.5 fuzzing levels 40,16,0 and 40,13,2, respectively, formed the variational basis in the case of paths with A_{1g} symmetry. A three-state basis may be expected to give a reasonable signal for the A'_{1g} excitation by reducing the contamination from higher excitations with this symmetry. For paths with E_u symmetry the fuzzing levels 16,13 were used for the two β's with two different transverse extents of the paths forming a variational basis. These transverse extents were one and two lattice spacings for small longitudinal lengths and one and four lattice spacings for larger R's. In order to set the scale, the lattice steps $a(2.4)$ and $a(2.5)$ were determined by fitting the two-body parametrization

$$V(R)=-\left[\frac{e}{R}\right]_L+b_S R+V_0 \tag{2.1}$$

TABLE I. Lattice spacing a determined using different methods.

β	$c=1.65$	$c=2.44$	$\sqrt{b_S}=440$ MeV
2.4	0.1098(5)	0.1183(5)	0.1190(5)
2.5	0.0778(4)	0.0839(4)	0.0846(4)
$\rho\equiv a(2.4)/a(2.5)$	1.412(14)	1.410(13)	1.406(11)

to measured potentials at interquark separations $R=2,3,4,6,8$, $R=2,3,4,6,12$ at $\beta=2.4, 2.5$, respectively. Here $[1/R]_L$ is the latticized form of the Coulomb potential $1/r$ due to one-gluon exchange. The above range of R was chosen to correspond to similar physical distance ranges. The usual method for estimating the lattice spacing is to equate the dimensionless value of b_S from the fit of Eq. (2.1) to an experimental value. This is equivalent to utilizing $V(R)$ in the limit $R\to\infty$. However, our experimental knowledge of the two-quark potential comes from heavy mesons with rms radii around 1 fm. An alternative method due to Sommer [9] compares the force from $V(R)$ to experimental values at a distance range more appropriate to these mesons, i.e., $r\approx 0.5$ fm. In practice the equation $(R_0)^2F(R_0)=c$ is used to find R_0, where $F(r)$ is the force between two static quarks at separation r. Various nonrelativistic continuum potential models give $aR_0\approx 0.49$ fm for $c=1.65$ and $aR_0\approx 0.66$ fm for $c=2.44$ [8]. The resulting scales and ratios of lattice spacings $\rho\equiv a(2.4)/a(2.5)$ are shown in Table I. The values of ρ from b_S and Sommer's scheme are seen to agree.

The $\beta=2.5$ potentials above have the accurate interpolations

$$V(R)_{A_{1g}}=0.555+0.0343R-0.280/R, \tag{2.2}$$

$$V(R)_{E_u}-V(R)_{A_{1g}}=3.8/R-12.6/R^2+24.6/R^3-18.8/R^4, \tag{2.3}$$

$$V(R)_{A'_{1g}}-V(R)_{A_{1g}}=5.94/R-23.6/R^2+49.2/R^3-38.8/R^4. \tag{2.4}$$

The relations are valid for $2\leqslant R\leqslant 12$, with no physical interpretation intended for the $V(R)_{E_u}$ and $V(R)_{A'_{1g}}$ expressions. The χ^2 values per degree of freedom are 0.09, 1.35, and 0.22 for the A_{1g}, E_u, and A'_{1g} states, respectively. The corresponding potential fits for $\beta=2.4$ are given in Ref. [1].

Our variational basis is constructed from fuzzed link operators that represent creation or annihilation of two quarks at separation R, with the color field in a specific state of lattice symmetry. These operators can be expanded in terms of the eigenstates of the transfer matrix

$$|R\rangle=c_0|V_0\rangle+c_1|V_1\rangle+\cdots, \tag{2.5}$$

with the measured correlation of a generalized Wilson loop given by

$$W(R,T)=\langle R_0|R_T\rangle=c_0^2e^{-V_0T}[1+|h(T/2)|^2+\cdots], \tag{2.6}$$

where

TABLE II. Excited-state contamination at $\beta=2.5$ as measured by $|h|$.

R	State	$t=1$	$t=2$	$t=3$
2	A_{1g}	0.012	0.005	
3	A_{1g}	0.027	0.012	0.009
4	A_{1g}	0.036	0.016	0.008
6	A_{1g}	0.073	0.034	0.016
12	A_{1g}	0.162	0.075	0.006
2	E_u	0.282	0.152	0.105
3	E_u	0.253	0.131	0.105
4	E_u	0.250	0.126	0.076
6	E_u	0.255	0.123	0.045
12	E_u	0.427	0.263	0.189
2	A'_{1g}	0.201	0.080	0.076
3	A'_{1g}	0.228	0.098	0.070
4	A'_{1g}	0.261	0.116	0.122
6	A'_{1g}	0.333	0.155	0.157
12	A'_{1g}	0.518	0.241	0.204

$$h(t)=\frac{c_1}{c_0}\,e^{-(V_1-V_0)t}. \tag{2.7}$$

To minimize excited-state contamination we need $h\ll 1$.

As plaquettes in the middle of the generalized Wilson loop in the time direction are used to probe the color fields, the relevant estimate of contamination is taken at $t=T/2$. The measured correlation is $\langle R_0|\Box_t|R_T\rangle$ instead of Eq. (2.6). This produces off-diagonal terms such as $\langle V_1|\Box_t|V_0\rangle$ that increase the coefficient of excited-state contribution from h to $2h$ for $T=2$, $t=1$. From the generalized Wilson loop ratios at each R value, we define $V(T)=-\ln[W(T)/W(T-1)]$ since its rate of approach to a plateau as $T\to\infty$ enables us to estimate the excited-state contamination to the ground state. We calculate h from

$$\begin{aligned}|h(t=T/2)|&\approx\frac{\lambda}{\lambda-1}\,\sqrt{V(T-1)-V(T)}\\&=\lambda\,\frac{V(T-1)-V(T\to\infty)}{\sqrt{V(T-1)-V(T)}}.\end{aligned} \tag{2.8}$$

Here the $T\to\infty$ extrapolated potential is defined as

$$V(T\to\infty)\equiv V(T)-\lambda\,\frac{V(T-1)-V(T)}{1-\lambda},\quad \lambda\equiv e^{-(V_1-V_0)}.$$

In practice λ was calculated from potentials at $T=1$. Table II shows the excited-state contamination for states of the two-body potential at $\beta=2.5$. It is seen that the A_{1g} states are reasonably pure with the E_u and A'_{1g} states containing increasing amounts of contamination. Note that the method used to extract the higher-excited-state contamination h to the first excited A'_{1g} state is unreliable since ground-state contributions can dominate in principle.

III. COLOR FIELD DISTRIBUTIONS

Color field distributions measured on a lattice are expected to be related to the physical continuum distributions. However, the finite spacing and changing physical size of the elementary square used to probe the fields introduce various artifacts, which will be discussed below. Our study of the field distribution around two static quarks consists of three types of observables. Three-dimensional sums over the spatial lattice to be presented in Sec. III A are used to extract β functions. Two-dimensional sums over the planes perpendicular to the interquark axis presented in Sec. III B show the longitudinal profile of the flux tube. This allows us to see the lattice self-energies and look for stringlike features in the remaining part. Our most microscopic observables are the transverse profiles of the flux tubes at the midpoint between the quarks, presented in Sec. III C. These show the clearest differences between ground and excited states and can be compared with models.

An important topic in this section is to check the quality of the input data for the sum rules by looking at their scaling properties between $\beta=2.4$ and 2.5. Essentially the input data are of two distinct forms: the two-quark potential V and the spatial sums of the color fields. In the past the scaling properties of V have been confirmed many times and will not be repeated here. However, scaling of the different color field combinations is less clear since the color fields are measured using a plaquette, whose physical size changes with β. This is relevant because only observables with the same physical size at different values of the coupling have a continuum limit. In the case of the three-dimensional sums over the color fields, the lattice sum rules provide the appropriate normalization as $a\to 0$. Even in this case, the scaling behavior is only known after the divergent self-energies are subtracted. However, other observables, such as the two-dimensional sums over transverse planes or the transverse profiles of the flux tube, do not have a well-defined scaling behavior, but it is still of interest to explore how similar the profiles are at the two values of coupling used.

From the relations in Eq. (1.2) and sum rules to be presented in Eqs. (4.1)–(4.3) we can see that the measured action sums must be multiplied by the anomalous dimension b/β to get the physical value, while the energy sums have a correction f that goes to one in the continuum limit. Here b,f are generalized β functions to be discussed later. As will be seen in Sec. IV below, the differences in the values of b and f between $\beta=2.4$ and 2.5 are sufficiently small to neglect them in the following plots; e.g., $b(2.4)/b(2.5)=0.97(7)$. Thus the normalization of the overall three-dimensional sum over color flux can be treated as almost constant in our β range. In turn this implies that we should compare more differential distributions using this scale.

A. Spatial sums

In Figs. 1–3 the three-dimensional spatial sums of the action S and longitudinal and transverse energies E_L, E_T involved in the sum rules are plotted as a function of R and T for the flux-tube ground state A_{1g} and the two excited states E_u and A'_{1g} for $\beta=2.5$ and the scaled data at $\beta=2.4$. The basic data $(\mathcal{E},\mathcal{B})$ are dimensionless and require the factor β/a^4 to give energy and action densities in GeV/fm^3. Since

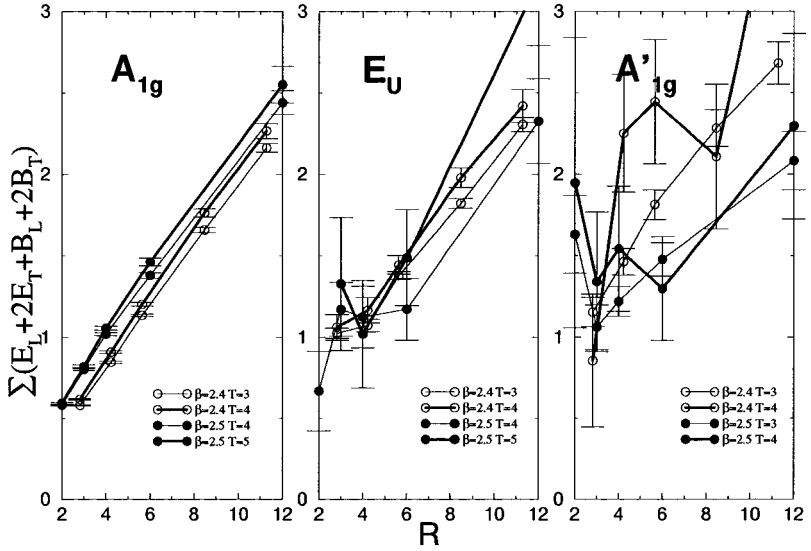

FIG. 1. Scaling of action (S) summed over the spatial lattice for paths with A_{1g}, E_u, and A'_{1g} symmetries.

Figs. 1–3 show the volume integrals of the basic data with $\beta=2.5$, for a scaling comparison, the volume integrals of the basic data for $\beta=2.4$ are multiplied by $2.4/2.5\rho$, where ρ is the ratio of lattice spacings given in Table I. The resulting two sets of data $[\beta=2.4(\text{scaled}),2.5]$ should not be expected to lie on top of each other since they have self-energies and self-actions that diverge as g^2/a from one-gluon exchange in leading-order perturbation theory. However, the two sets of data should be parallel to each other since the self-energies are independent of R. In the following extraction of the β function, it is the extent to which the *slopes* of these lines are *nonzero* that is relevant.

In Figs. 1–3, for clarity, only the data for one or two T values are drawn. The data for higher T have larger errors, but in most cases they are consistent with the data shown, indicating that the plateau in T is achieved. In Fig. 1, for the action, the A_{1g} and E_u states show scaling and with distinct nonzero slopes. This is best seen for the A_{1g} state and deteriorates progressively in going to the E_u and A'_{1g} states. Scaling is questionable for the latter. Even so, the action and its R dependence are comparable in all three cases. A very approximate estimate of the difference ΔS_0 in the $\beta=2.5$ and $\beta=2.4(\text{scaled})$ self-actions is given by the vertical difference between the two sets of data. The result given by linear fits for the A_{1g} ground state, $\Delta S_0\approx 0.12(2)$, is not inconsistent with the E_u case, whereas the A'_{1g} excitation has a positive self-action difference only for the smallest R's. This curious feature of the A'_{1g} data is perhaps not surprising since already Table II shows that this state has considerable contamination from other states. However, in spite of this, we thought it useful to include such data in this paper to illustrate where the data need to be improved.

In Fig. 2, for the longitudinal energy, the data are an order of magnitude smaller than for the action. Here the dependence on β is less clear and the presence of a nonzero slope much less distinct for the E_u and A'_{1g} cases. The difference ΔE_0 in the $\beta=2.5$ and $\beta=2.4(\text{scaled})$ self-energies is now best taken visually at the lowest R's, giving $\Delta E_0\approx 0.020(5)$

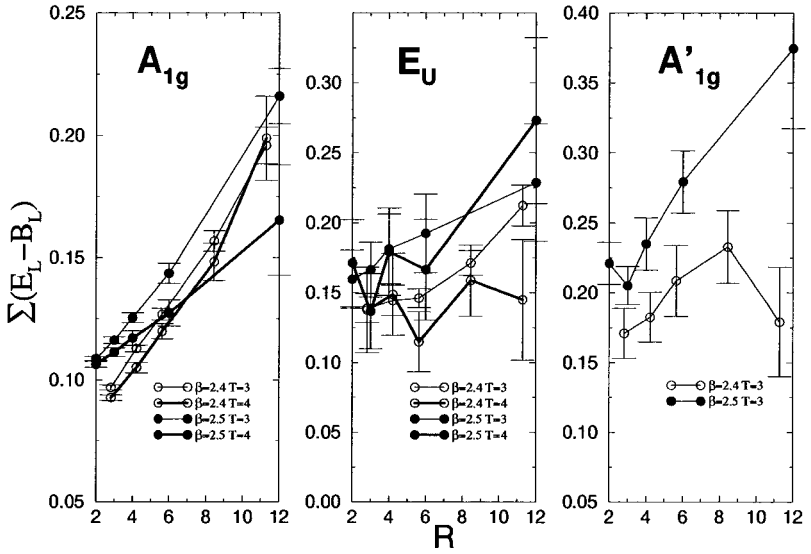

FIG. 2. Scaling of longitudinal energy (E_L) summed over the spatial lattice for paths with A_{1g}, E_u, and A'_{1g} symmetries.

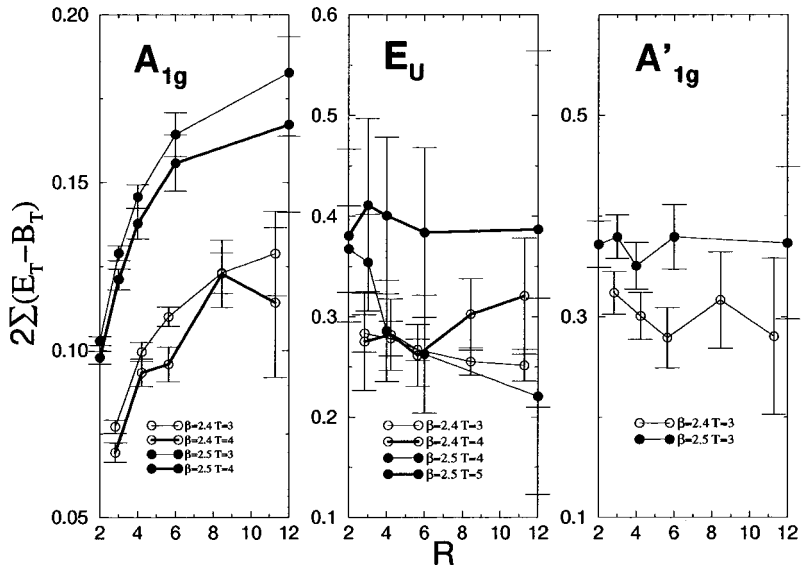

FIG. 3. Scaling of transverse energy (E_T) summed over the spatial lattice for paths with A_{1g}, E_u, and A'_{1g} symmetries.

for the A_{1g} state. The data for the gluonic excitations are consistent with this estimate. For A_{1g} the curves cross at $R=6$ and at higher R's the $\beta=2.4$ curve lies higher.

In Fig. 3, for the transverse energy, only the A_{1g} state shows a slope that is slightly nonzero, with both the E_u and A'_{1g} cases having slopes consistent with zero. However, there is a distinct self-energy effect with $\Delta E_0 \approx 0.04(1)$ for the A_{1g} state, again consistent with the gluonic excitations. Since it is the presence of nonzero slopes that is relevant for extracting the β function, Figs. 2 and 3 already indicate that problems will arise when attempting to utilize the $E_{L,T}$ data.

B. Transverse sums

The self-energy differences in the above spatial sums can be seen much more clearly in the transverse sums shown in Figs. 4–6, where the longitudinal dependence of the sum over R_L is presented for paths with A_{1g}, E_u, and A'_{1g} symmetries and interquark separation $R=8,12$ at $\beta=2.4,2.5$, respectively. In these figures, $R_L=0$ corresponds to the midpoint of the interquark separation, while $R_L=R/2$ corresponds to the position of the static quark sources. The R values were chosen to correspond to approximately the same physical distance at these two couplings, namely, 0.946(4) and 1.007(5) fm. The plotted data are taken at $T=3$, where we have a good signal-to-noise ratio. Unfortunately, this means that the excited-state contamination is relevant at $T=1,2$, where h is largest, as can be seen from Table II. Furthermore, we are also using the largest R's, where the excited-state contamination becomes quite significant especially for the E_u and A'_{1g} cases.

These transverse sums do not, strictly speaking, have a continuum limit. However, in string models the transverse sums near the center of long strings should be independent of R so that, to the extent that string models are applicable and that R is sufficiently large, scaling would be expected. This is the assumption made in presenting the data in earlier works [10]. In the figures, the basic $\beta=2.5$ data are compared with the basic $\beta=2.4$ data, which have been multiplied by $2.4/2.5\rho^2$. The longitudinal energy is plotted at half-integer lattice spacings (i.e., averaging over neighbouring values of $\mathcal{E}_T, \mathcal{B}_L$ instead of $\mathcal{E}_L, \mathcal{B}_T$) to get a better determination of the self-energy peak. In this case these peaks are expected to diverge as g^2/a^2 in physical units.

Figure 4 shows for the A_{1g} state that, within error bars, all three field combinations (action, E_L, and E_T) scale well near the center of the flux tube ($R_L=0$). However, near the quarks ($R_L \approx 6$ in this case) the $\beta=2.4$ and 2.5 curves differ considerably. This is mainly the effect of the self-energies being seen. These data near $R_L=6$ shows some interesting features.

(a) Except for the $\beta=2.4$ action, all the data exhibit a distinct peak near $R_L=6$ and the $\Delta S_0, \Delta E_0$ extracted from Figs. 1–3 are qualitatively consistent with the corresponding

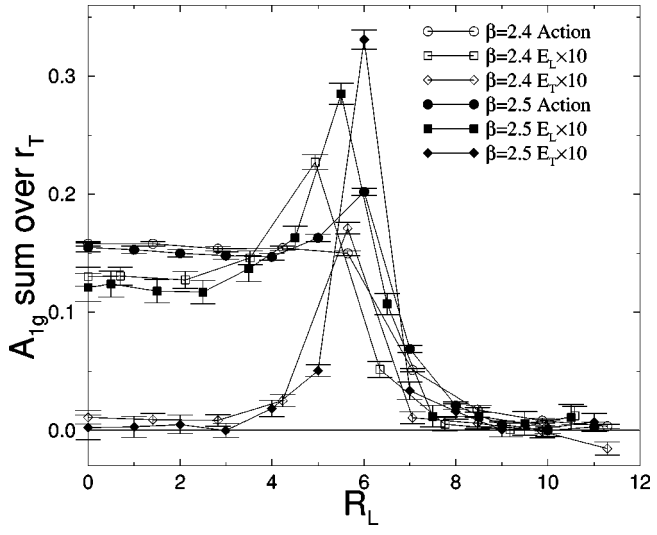

FIG. 4. Dependence on longitudinal position (R_L) of the sum over the transverse plane of the color flux contributions corresponding to the action, longitudinal (E_L), and transverse energy (E_T) sum rules of Eqs. (4.1)–(4.3). Here R_L is measured from the midpoint for separation $R=8,12$ at $\beta=2.4,2.5$, respectively. The data are in units of $a(2.5)$ for the symmetric ground state (A_{1g} representation) at $T=3$.

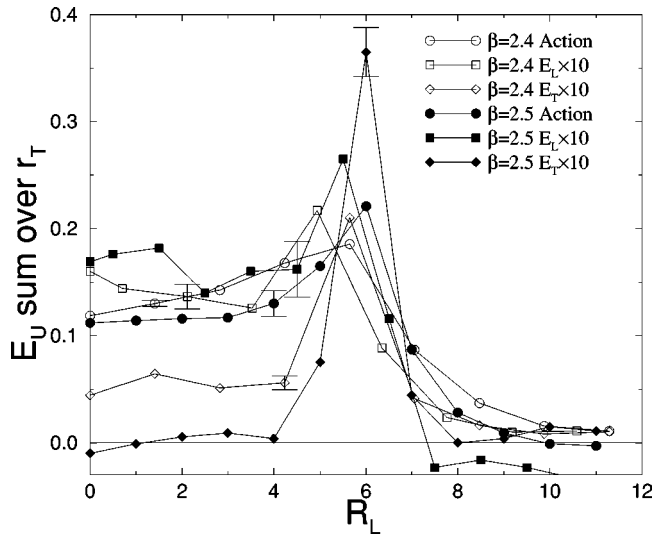

FIG. 5. Same as in Fig. 4, but for the first gluonic excitation (E_u representation). For each data set one error bar is shown; others are similar.

values estimated from the areas under these peaks. We can estimate the self-energy peak height by subtracting the value at $R_L=0$ from the value at $R_L\approx 6$. For the action sums at 2.4 we cannot see any self-energy peak, while for E_L the ratio of self-energy peak heights at $\beta=2.4$ and 2.5 is 0.59. For E_T the peak height ratio is somewhat lower at 0.49; this will be discussed below.

(b) The transverse energy E_T is completely dominated by the self-energy with the latter being at least an order of magnitude larger than the non-self-energy terms, which are expected to be essentially independent of R_L between the two quarks. This immediately explains the small slope of the A_{1g} curve in Fig. 3. It also shows that any volume integral of the self-energy contribution cannot be accurately evaluated on the present lattice since, in the $\beta=2.5$ case, the $R_L=6$ contribution is an order of magnitude larger than those from $R_L=5,7$ i.e., the whole volume integral is given by contributions (each with $\approx 10\%$ errors) from only *three* values of R_L. Therefore, when the volume integrals from different values of R are subtracted, it will be hard to get a meaningful signal for the R dependence of interest.

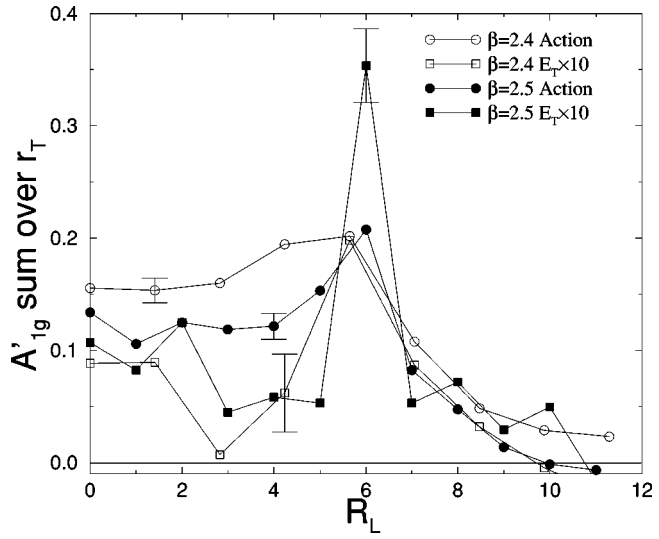

FIG. 6. Same as in Fig. 4, but for the second gluonic excitation (A'_{1g} representation). For each data set one error bar is shown; others are similar.

In principle, the self-energy contribution can stretch out to the midpoint between the two quarks. According to our data, for the largest interquark separations as shown here, any such contribution seems negligible. This is seen by looking at the data near $R_L\approx 10-12$, which should be dominated by any self-energy tail. However, for the smaller R's the transverse sums at the midpoint can well have significant self-energy contributions, which is seen in later in Sec. IV C when these data are used to determine β functions.

(c) The trend is that, for the action, the peak is about a 5% effect compared to the plateau contribution from $R_L=0,\ldots,6$, for E_L the peak is about 50% of the plateau contribution, and for E_T the peak completely dominates. Therefore, it should be expected that any predictions that depend on canceling the self-energies are most reliable for the action and least for E_T.

In Fig. 5 the corresponding transverse sums are shown for the E_u state. The most notable features are the following.

(a) The action and E_L both scale within error bars for $R_L\approx 0$.

(b) As expected, the $\beta=2.4$ data show, for $R_L\approx 0$, an enhancement of E_T over its A_{1g} counterpart, whereas the action and E_L are comparable to the A_{1g} data. However, this enhancement in E_T is not seen for $\beta=2.5$, but this could be due to the relatively large errors for this case.

(c) Again the action for $\beta=2.4$ does not exhibit a distinct peak near $R_L=6$. Instead it simply shows a monotonic increase as R_L goes from 0 to 6. The ratio of self-energy peak heights is 0.61,0.59 for the action and E_L, respectively, the latter being the same as in the A_{1g} case. For E_T the ratio is 0.46, lower than for E_L by an amount similar to that observed for A_{1g}.

(d) Compared with S and E_L, E_T has a self-energy that is comparable to or larger than the plateau contribution from $R_L=0,\ldots,6$.

In Fig. 6 the data for the A'_{1g} state is shown with the following features.

(a) The action and E_T are approximately scaling within the rather large error bars. However, for E_L (not shown) it is not possible to make this claim since the error bars are too large.

(b) The E_T data, unlike that in the E_u case, now exhibit some enhancement, compared to the A_{1g} state, for *both* $\beta=2.4$ and 2.5. For example, at $\beta=2.4$ and $R_L=0$, $E_T(A_{1g})\approx 0.01(1)$, $E_T(E_u)\approx 0.04(1)$, and $E_T(A'_{1g})\approx 0.09(5)$. Even so, the plateau terms are still, at most, only comparable to the self-energies. Therefore, as for the A_{1g} and E_u cases, those predictions that require a delicate cancellation of the self-energies are possibly not reliable.

We observed faster divergence of the transverse component of the self-energy than the longitudinal one for the A_{1g}, E_u states in Figs. 4 and 5. As the self-energies should be isotropic, the difference in the peak height ratios at the two β's is worth exploring further.

This difference is caused by the different discretization of longitudinal and transverse plaquettes. The electric field is

dominant, so E_T is mainly composed of plaquettes lying in the transverse plane, whereas E_L is mainly a planar sum of plaquettes with a perpendicular orientation. A simple way to investigate their diverging behavior is to consider a scalar field $\phi = e^{-b|r|}$ with $b \approx 10$/fm and the integrals over it analogous to our sums. The (normalized) integral over the transverse two-dimensional plane, where the source lies, is found to change faster when the lattice spacing is varied than the integral over a three-dimensional ''slice'' of width a, analogous to E_L. For our $a(2.4)$ and $a(2.5)$ the ratio [plane(2.4)/plane(2.5)]/[slice(2.4)/slice(2.5)]≈ 0.8 (also for $\phi = e^{-b^2|r|^2}$), which agrees with the corresponding ratio observed for the E_T and E_L for paths with A_{1g} and E_u symmetries. The lower-peak-height ratios for E_T and the high ΣE_T peaks observed in Figs. 4–6 are also due to this effect.

The diverging of the transverse sums over color sources is quite consistent with the expectation from leading order perturbation theory; $[2.5a(2.5)^2]/[2.4a(2.4)^2] = 0.52(1)$ is in the middle of the values observed. This suggests that the peaks are dominated by lattice self-energy effects. E_L diverges slower than the perturbative expectation, as expected, because of the transverse extent of the dominant electric field. On the other hand, for E_T we would expect g^2/a^2 behavior, while the observed peak height ratios diverge slightly faster than this.

C. Transverse profiles

In Figs. 1–6 the scaling properties of the three-dimensional (3D) volume and, assuming the flux tubes have stringlike features, of the 2D transverse integrals are demonstrated, with some combinations of the color fields being more successful than others in satisfying this property. It is therefore of interest to proceed finally to the ''scaling'' properties of the individual flux-tube profiles. The transverse dependence of the action (S) and longitudinal and transverse energies ($E_{L,T}$), measured at the midpoint ($R_L = 0$ in our convention) with the separations $R = 8,12$ at $\beta = 2.4,2.5$, respectively, is presented in Figs. 7–9. The correlations shown were measured at $T = 3$ for the Wilson loop. As we are again using a small T and large R, excited-state contamination is significant in the E_u and A_{1g}' cases. Here the $\beta = 2.4$ data are compared with the $\beta = 2.5$ data by multiplying the former by $2.4/2.5\rho^4$.

Aside from any intrinsic nonscaling arising from the different scale of the plaquette used to probe the flux distributions, we should also be aware that effects can arise from the discretization versus R_T of the distribution and possibly from self-energy effects. We have found earlier that the self-energy effects are negligible at the midpoint ($R_L = 0$) in the integrated distributions. We here assume that this applies to the differential distributions so this contribution can be neglected. The effect of the discretization in R_T is that a sharply peaked distribution will be suppressed at coarser lattice spacing. There is some sign of this latter effect in our data: The smaller plaquette at $\beta = 2.5$ should increase the observed height of peaks (such as the center of the flux tube $R_T = 0$ in the A_{1g} case), whereas at the smoother regions (away from the center in the A_{1g} case) the shapes at the two β's should be more similar to each other. This is indeed observed; in the E_u case, the largest differences are at $R_T \approx 2$

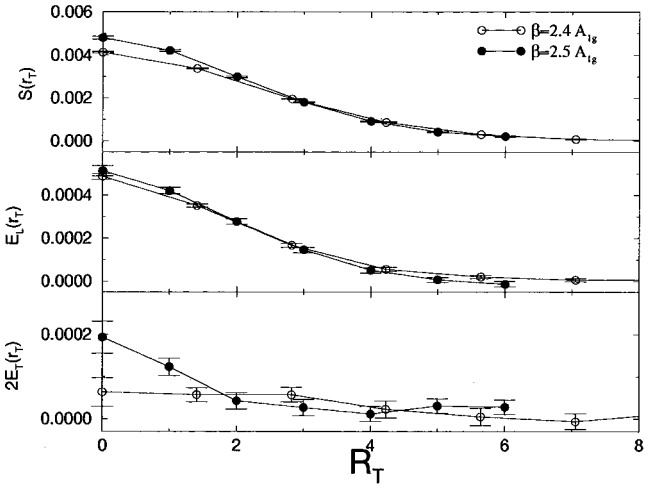

FIG. 7. Color flux contributions corresponding to the action (S), longitudinal (E_L), and transverse energy (E_T) sum rules of Eqs. (4.1)–(4.3) for the static quark potential. These are shown in units of $a(2.5)$ versus transverse distance R_T at the midpoint ($R_L = R/2$) for separation $R = 8,12$ at $\beta = 2.4,2.5$. The data are for the symmetric ground state (A_{1g} representation).

or 3 instead of $R_T = 0$ as for the A_{1g} symmetry because the distributions peak at these values. This effect has not been mentioned in earlier works [10,11].

Assuming some function describing the continuum density, we could apply a discretization procedure, e.g., simply averaging over cubes of volume a^3, that simulates the flattening of the peaks in our finite-a simulations. The latticized continuum function could then be fitted to measured points. When this procedure is applied at both simulated values of the lattice spacing, we would get two corrected parametrizations. If these two agree, this then would suggest that this transverse distribution would apply in the continuum limit. This would be the way to compare with continuum models of the flux tube. Previously, we have found qualitative agreement [1] with the dual QCD model of Refs. [12, 13] for the A_{1g} profiles.

In the present case, it appears at first sight that the only cases where the results for the two β's are consistent are

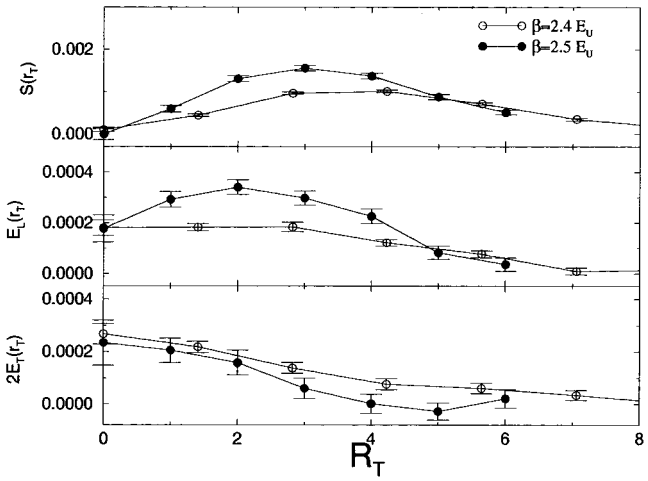

FIG. 8. Same as Fig. 7, but for the first gluonic excitation (E_u representation).

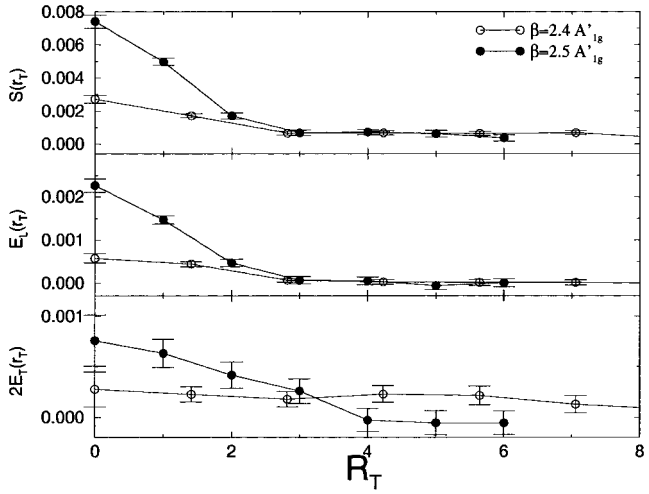

FIG. 9. Same as Fig. 7, but for the second gluonic excitation (A'_{1g} representation).

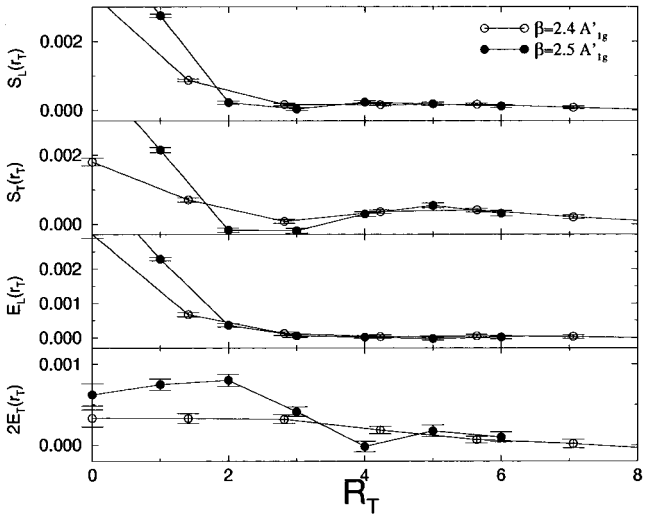

FIG. 10. Same as Fig. 9, but with longitudinal and transverse components of the action presented separately and for interquark separation $R=4,6$ at $\beta=2.4,2.5$, respectively.

$S(A_{1g})$ and $E_L(A_{1g})$, whereas in the 2D sums of Figs. 4–6 other cases, such as $S(E_u),E_L(E_u)$ and even $S(A'_{1g}),E_T(A'_{1g})$, seem to show reasonable scaling. The possible reasons for this are twofold.

(i) Figures 7–9 only show the profile in a single direction, along a lattice axis, whereas Figs. 4–6 are an average over all directions in a plane. In particular, this could have an effect on small values of R_T, where rotational invariance is most violated.

(ii) The curves depicted in Figs. 7–9 must be multiplied by a phase space factor $2\pi R_T dR_T$ when their contributions to any 2D sum rule are estimated. Therefore, the values near $R_T\approx 0$ get drastically reduced and, in the A_{1g} and A'_{1g} cases, it is this region of R_T that is varying the most with β.

An interesting feature in the A'_{1g} profiles is a local minimum (a dip) outside the center of the tube as predicted by the $N=1$ Isgur-Paton model [14] for the energy density. In Fig. 9 the action can be seen to have a plateau at $3\leqslant R_T\leqslant 5$ unlike in the A_{1g} case. For E_L no evidence of a dip is found, whereas for E_T the data with $\beta=2.4$ hint at a minimum for $R_T\approx 3$ with the $4\leqslant R_T\leqslant 7$ values being above zero unlike the A_{1g} case, which is consistent with zero for $R_T\geqslant 4$.

A better statistical accuracy is achieved in the transverse profiles of flux tubes with interquark separation $R=4,6$ at $\beta=2.4,2.5$, respectively, corresponding to interquark distances of 0.473(5) and 0.503(7) fm. These are shown in Fig. 10 with the longitudinal and transverse components of the action plotted separately. There is now a clear dip in the transverse action profile, again at $R_T\approx 3$, with a corresponding maximum at $R_T\approx 5$. A similar dip and maximum are seen in the longitudinal action at $\beta=2.5$, whereas the $\beta=2.4$ data have a plateau at $3\leqslant R_T\leqslant 6$. As in Fig. 9, no evidence for a dip is found for E_L, whereas the E_T data show a clear dip at $\beta=2.5$ with a minimum at $R_T=4$. At $\beta=2.4$ there is no minimum, but the decay as a function of R_T is slow, the value at $R_T\approx 6$ being an order of magnitude higher than in the corresponding A_{1g} case. However, again it should be emphasized that Table II indicates for the A'_{1g} state considerable contamination from neighboring states. Therefore, any nodal structure possibly present in a pure A'_{1g} state could well be smoothed out by interference effects. Also, it should be added that the Isgur-Paton model, which suggests such dips, is less applicable for these smaller values of R.

IV. DETERMINATION OF β FUNCTIONS FROM SUM RULES

After presenting the results from our simulations in the previous two sections we are now ready to embark on the extraction of the lattice β functions using these data. This will be done in three ways, which have different sources of systematic and statistical errors. Method 1 in Sec. IV A is the most straightforward, while method 2 in Sec. IV B attempts to eliminate systematic errors from a discrete derivative. The limit of large quark separation to be studied in Sec. IV C is connected with string models. Finally, a brief review of the best estimates of β functions in SU(2) lattice gauge theory is given in Sec. IV D.

In Ref. [5], by imposing the condition on the interquark potential V that $\partial V(R)/\partial a|_R=0$, the following three sum rules were derived relating V to spatial sums of the electric and magnetic color:

$$\frac{-1}{b}\left(V+R\,\frac{\partial V}{\partial R}\right)+S_0=\sum S = -\sum\,(\mathcal{E}_L+2\mathcal{E}_T+2\mathcal{B}_T+\mathcal{B}_L), \tag{4.1}$$

$$\frac{1}{4\beta f}\left(V+R\,\frac{\partial V}{\partial R}\right)+E_0=\sum E_L=\sum\,(-\mathcal{E}_L+\mathcal{B}_L), \tag{4.2}$$

$$\frac{1}{4\beta f}\left(V-R\,\frac{\partial V}{\partial R}\right)+E_0=\sum E_T=\sum\,(-\mathcal{E}_T+\mathcal{B}_T). \tag{4.3}$$

Here the generalized β functions are defined considering an asymmetric lattice as in Ref. [15]. In the notation of Ref. [5], they are $b\equiv\partial\beta/\partial\,\ln a=2(S+U)$ and $f\equiv(U-S)/2\beta$. In Eqs.

(4.1)–(4.3), S_0 and E_0 are the self-action and -energy associated with the quarks and are therefore independent of R. The same self-energy E_0 is expected for both orientations (L and T) of the color electric field.

The three-loop perturbative expression for b in terms of $\alpha = g^2/4\pi = 1/\pi\beta$ is $b = -0.371\,51(1 + 0.491\,93\alpha - 0.9795\alpha^2 + \cdots)$. On the other hand, for f we have $f = 1 - 0.456\pi\alpha - 0.25\pi\alpha b + \cdots$, where we can insert the expression for b giving $f = 1 - 1.1408\alpha + \cdots$.

The aim is to now extract estimates of b and f in the nonperturbative situation encountered in practice. This will be carried out in various ways, each of which has its own advantages and disadvantages. However, their common feature is that, on the left-hand side of each sum rule, the potential V is measured on the lattice using Wilson loops $W(R,T)$ and, on the right-hand side as discussed in the introduction, the color fields $\mathcal{E}$ and $\mathcal{B}$ at a point r are measured using Eq. (1.1) involving the same loops. Unfortunately, this strategy is complicated by two features in Eqs. (4.1)–(4.3). First, the self-energies are unknown and so their effect must be removed by considering differences between the equations for different values of R, or for different gluonic states $A_{1g}, E_u, \ldots$ with the same R, a possibility not considered here. Second, each equation contains $\partial V/\partial R$. Even though the potential V itself can be readily determined as a by-product of the $\mathcal{E},\mathcal{B}$ measurement on a lattice, the determination of $\partial V/\partial R$ introduces some uncertainty. All of the estimates in this section are made using the A_{1g} ground state, where we have the best signal. The other gluonic states have such large errors that sensible values of b, f cannot be extracted.

A. Method 1: Fitting the sum rules

The most direct approach is to measure $\mathcal{E}$ and $\mathcal{B}$ over all space and to then perform the spatial sum giving the right-hand side of Eqs. (4.1)–(4.3). In practice, ''spatial sum'' means a sum over a lattice that has a linear size twice that of the maximum R considered, i.e., for $\beta = 2.4$ (2.5) up to $R = 8$ (12) on lattices with spatial size 16^3 (24^3). With V known numerically from Eq. (2.1), the derivative can also be estimated. The function b is then obtained using Eq. (4.1) by plotting $\Sigma(\mathcal{E}_L + 2\mathcal{E}_T + \mathcal{B}_L + 2\mathcal{B}_T)$ vs $V(R) + R[\partial V(R)/\partial R]$ and performing a linear fit, as shown in Fig. 11. The $R = 1$ points were not included in the fits due to the artifacts they contain, while the $R = 12$ point at $\beta = 2.5$ was excluded because of its significant excited-state contamination (see Table II). There are four sets of data for each β corresponding to the correlation of the sum over electric and magnetic fields taken at time intervals $T = 3,\ldots,6$. The $\beta = 2.4$ data were scaled by multiplying with $2.4/2.5\rho$ to have the same units as the $\beta = 2.5$ plots. The results of the fit in Fig. 11 can be read from the second column of Table III.

For $\beta = 2.4$ the function b has reached a plateau at $T = 5$, giving a best estimate of $-0.312(15)$, whereas for $\beta = 2.5$ a plateau has been reached only at $T = 6$ with $-0.323(9)$ being our best estimate. The self-energy estimates S_0 are also seen to reach plateaus at $-1.2(1)$ and $-1.5(1)$ for $\beta = 2.4, 2.5$, respectively.

Even though the $\beta = 2.4$ and 2.5 lines in Fig. 11 are almost parallel as in Fig. 1, they are separated by the difference in their self-energies. The strategy of fitting the data with a straight line is effectively taking differences of Eq. (4.1) evaluated for different values of R and so avoids the need to know S_0 explicitly.

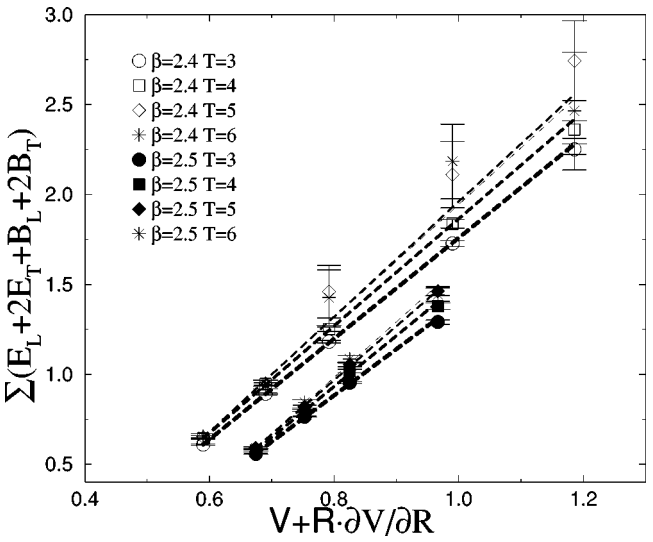

FIG. 11. Data corresponding to Eq. (4.1) with best linear fits.

In principle, the function f can be extracted from either of the two sum rules in Eqs. (4.2) and (4.3). However, as shown in the fourth and sixth columns of Table III, these predictions exhibit much more variation and have much greater errors than those for b. The main reason for this is due to the larger variation of the sums of the *differences* of electric and magnetic fields. In particular, the values of $f(I)$ at $\beta = 2.4$, $T = 5,6$ and $\beta = 2.5$, $T = 4,5,6$ are essentially undetermined.

The self-energies E_0 are not consistent with zero for $f(I)$ at $\beta = 2.5$ as they are for $f(I,II)$ at $\beta = 2.4$ and $f(II)$ at $\beta = 2.5$. As E_0 is the difference of (i) $V_0/4\beta f$ coming from the two-body potentials in Eq. (2.1) and (ii) the self-energy in E_L, E_T for $f(I,II)$, respectively, we can see that these two cancel for all cases except $f(I)$ at $\beta = 2.5$. As the self-energies should be isotropic, this is probably caused by inaccuracies in determining ΣE_L.

This inaccuracy in determining f can be greatly reduced if the sum rules in Eqs. (4.2) and (4.3) are fit together. At $\beta = 2.4, 2.5$ data for the former sum rule are taken at $T = 3,4$ and $T = 3$, respectively, while for the latter the data can be taken at any T from 3 to 6. The function f obtained in this manner is presented in Fig. 12 and Table IV and can be seen to lead to a much more accurate estimate of f. Our best estimates are 0.65(1) and 0.68(1) at $\beta = 2.4, 2.5$, respectively. Also the values of self-energy are now more stable at $E_0 \approx 0.01(1)$, a number that is about two orders of magnitude smaller than the self-actions S_0.

In the above, the parameter ρ has been extracted and found to be 1.411(13). This then suggests as a direct estimate of b, averaged over the β range of 2.4–2.5, the value

$$b = \frac{\Delta\beta}{\Delta \ln[a]} = -\frac{2.5 - 2.4}{\ln[a(2.5)] - \ln[a(2.4)]} = -0.290(8).$$

Even though this is admittedly a very crude estimate, it should represent the average value of b over this range of β. However, it appears to be slightly smaller in magnitude than

TABLE III. Estimates for b and f at $\beta=2.4$, 2.5 at different T values.

β	T	b	S_0	f (I)	E_0	f (II)	E_0
2.4	3	−0.357(3)	−1.04(2)	0.63(3)	0.004(4)	0.63(5)	0.005(3)
	4	−0.336(5)	−1.11(3)	0.71(6)	0.010(7)	0.74(10)	0.007(4)
	5	−0.312(15)	−1.24(10)	1.5(1.3)	0.06(2)	0.84(28)	0.01(1)
	6	−0.317(21)	−1.21(14)	4.5(7.0)	0.09(4)	1.4(8)	0.02(2)
2.5	3	−0.389(4)	−1.17(2)	0.89(7)	0.033(7)	0.59(3)	0.002(3)
	4	−0.354(5)	−1.32(3)	1.41(23)	0.059(10)	0.64(5)	0.003(5)
	5	−0.333(7)	−1.44(4)	1.49(38)	0.063(16)	0.75(11)	0.011(8)
	6	−0.323(9)	−1.49(7)	6(11)	0.10(3)	0.74(16)	0.009(12)

the average of the above estimates $-0.312(15)$ at $\beta(2.4)$ and $-0.323(9)$ at $\beta(2.5)$. The origin of this two-sigma difference is not clear.

B. Method 2: Combining the sum rules

As shown in Ref. [6], one way to avoid estimating $\partial V(R)/\partial R$ and S_0, E_0 is to explicitly eliminate them by writing down Eqs. (4.1)–(4.3) for two different values of R. In this way

$$b=\frac{2[V(R_1)-V(R_2)]\left(1+\dfrac{\Sigma(E_T)_{R_1}-\Sigma(E_T)_{R_2}}{\Sigma(E_L)_{R_1}-\Sigma(E_L)_{R_2}}\right)^{-1}}{\Sigma S_{R_1}-\Sigma S_{R_2}}, \tag{4.4}$$

$$f=\frac{V(R_1)-V(R_2)}{2\beta[\Sigma(E_T)_{R_1}-\Sigma(E_T)_{R_2}+\Sigma(E_L)_{R_1}-\Sigma(E_L)_{R_2}]}. \tag{4.5}$$

At first sight this appears to be what is needed, expressions that involve quantities that can be measured directly. However, in practice, there is a problem: b becomes dependent on the differences $\Sigma(E_L)_{R_1}-\Sigma(E_L)_{R_2}$ and $\Sigma(E_T)_{R_1}-\Sigma(E_T)_{R_2}$ from Eqs. (4.2) and (4.3) and, as seen above, the values of these differences are less accurate than $\Sigma S_{R_1}-\Sigma S_{R_2}$. The outcome of this strategy is given in Fig. 13. There it is seen that the $b(2.4)$ results are consistent with those given by method 1, but have much larger error bars. However, the $b(2.5)$ results are essentially inconsistent with method 1. A similar problem arises with the values of f from Eq. (4.5). Again $f(2.4)$ is consistent with the earlier estimates of method 1 in Ref. [6], but with much larger error bars. For example, with $R_1, R_2=2,6$ we get $f(T=4,5)=0.64(7),0.64(15)$. However, compared to method 1, $f(2.5)$ is too large, rising to $\approx 0.9(2)$ at $T\approx 4,5$. It should be added that this is not a problem of the measurements being poorly distributed, since plotting the bootstrap values of b shows that the errors are not underestimates due to asymmetric non-Gaussian bootstrap distributions.

This difference between the two estimates of b for $\beta=2.5$ but not 2.4 is caused by the inaccurate determination of the longitudinal energy sums $\Sigma(E_L)_{R_1}-\Sigma(E_L)_{R_2}$ in Eq. (4.4). As can be seen in Fig. 2, for the ΣE_L curves at $\beta=2.5$ the slope is rather erratic and indicates a much smaller value

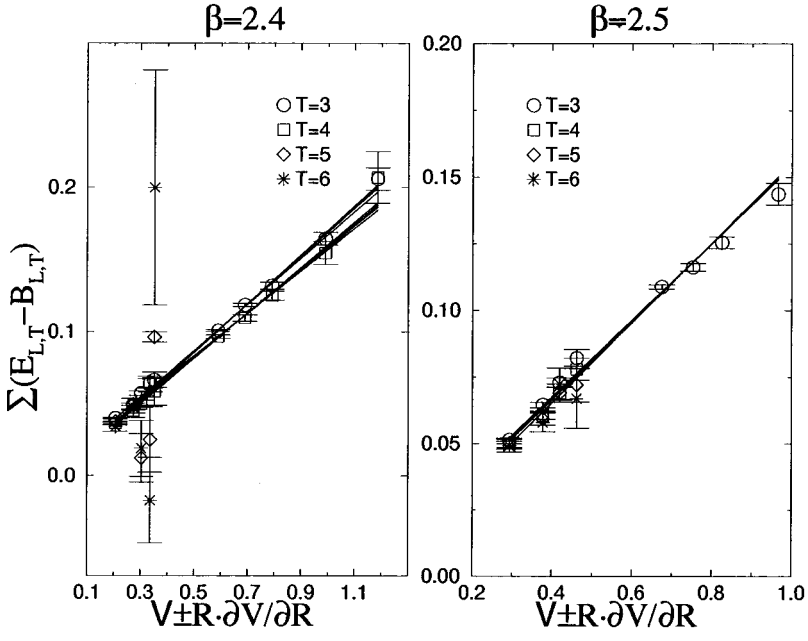

FIG. 12. Determination of $f(I+II)$ by combining two sum rules.

TABLE IV. Combined fits of f at $\beta=2.4,2.5$ at different T values. The first T value refers to the data used for Eq. (4.2), the other to the data used for Eq. (4.3).

β	T	$f(I+II)$	E_0
2.4	3,3	0.647(7)	0.006(1)
	3,4	0.616(8)	0.0008(10)
	3,5	0.627(17)	0.003(3)
	3,6	0.612(18)	0.013(4)
	4,3	0.705(13)	0.009(1)
	4,4	0.671(13)	0.004(1)
	4,5	0.684(23)	0.040(5)
	4,6	0.659(27)	0.030(6)
2.5	3,3	0.694(11)	0.010(1)
	3,4	0.667(11)	0.005(1)
	3,5	0.682(16)	0.008(2)
	3,6	0.688(21)	0.009(3)

than at $\beta=2.4$. This is also reflected in Table III, where the $f(I)$ value obtained using the ΣE_L values is already at $T=3$ unrealistically high for $\beta=2.5$, getting worse with increasing T. This means that the $\Sigma(E_L)_{R_1}-\Sigma(E_L)_{R_2}$ are underestimated. For ΣE_T the situation is more consistent, which can be seen in the larger slope in Fig. 3 and the reasonable behavior for the $f(II)$ in Table III at $\beta=2.5$. Thus $\Sigma(E_L)_{R_1}-\Sigma(E_L)_{R_2}$ is too small and $\Sigma(E_T)_{R_1}-\Sigma(E_T)_{R_2}$ realistic, leading to underestimates of $b(2.5)$ using Eq. (4.4) and an overestimate of $f(2.5)$ from Eq. (4.5). The signal being worse for E_L than E_T is somewhat surprising since it is E_T where the self-energy completely dominates. Therefore, one would have expected it to be harder to get a signal for E_T because it requires a more delicate cancellation of the self-energy.

Why does this not happen at $\beta=2.4$? From Figs. 2 and 3 we can see that the ΣE_L slope is larger and the ΣE_T slope slightly smaller than at $\beta=2.5$. This is again reflected in Table III, where $f(I)$ again gets larger with increasing T, but not as much as for $\beta=2.5$ and with larger errors making the estimates consistent with a realistic value. At the same time, unlike for $\beta=2.5$, $f(II)$ also increases. This fortuitously leads to a realistic ratio of the differences of the sums in Eq. (4.4) and a value of b consistent with method 1.

C. Method 3: The large-R limit

In the above, the derivatives of V are calculated numerically from the lattice form of the interquark potential in Eq. (2.1). However, for sufficiently large $R(R\geqslant 2)$, the continuum form of V (i.e., with $[1/R]_L$ replaced with $1/R$) is a good approximation. When, in addition to this, the effect of the self-energies is removed by evaluating the sum rules at two values of R, Eqs. (4.1)–(4.3) reduce to

$$b=\frac{-2b_S(R_1-R_2)}{\Sigma S_{R_1}-\Sigma S_{R_2}}, \tag{4.6}$$

$$f(I)=\frac{b_S(R_1-R_2)}{2\beta[\Sigma(E_L)_{R_1}-\Sigma(E_L)_{R_2}]}, \tag{4.7}$$

$$f(II)=\frac{-e(1/R_1-1/R_2)}{2\beta[\Sigma(E_T)_{R_1}-\Sigma(E_T)_{R_2}]}. \tag{4.8}$$

As seen in Fig. 14(a) for $\beta=2.5$, Eq. (4.6) gives estimates in agreement with the fits in Table III for $R_1,R_2=2,\ldots,12$. However, this is not surprising since there the results are an average over a range of R values, whereas Eqs. (4.6)–(4.8) can be considered as an average using simply two values of R. A similar situation holds for $\beta=2.4$.

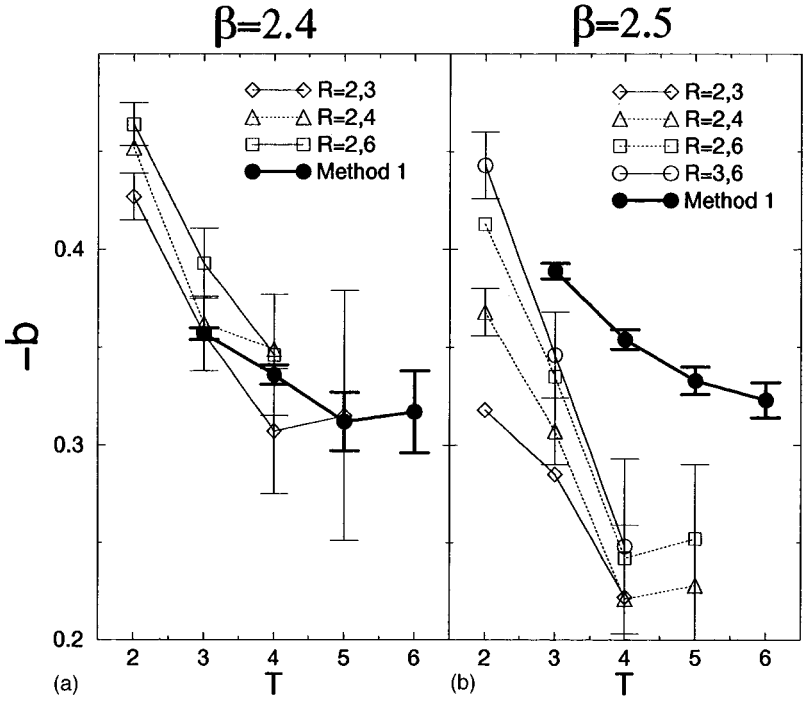

FIG. 13. Estimates of b from Eq. (4.4) for (a) $\beta=2.4$ and (b) $\beta=2.5$.

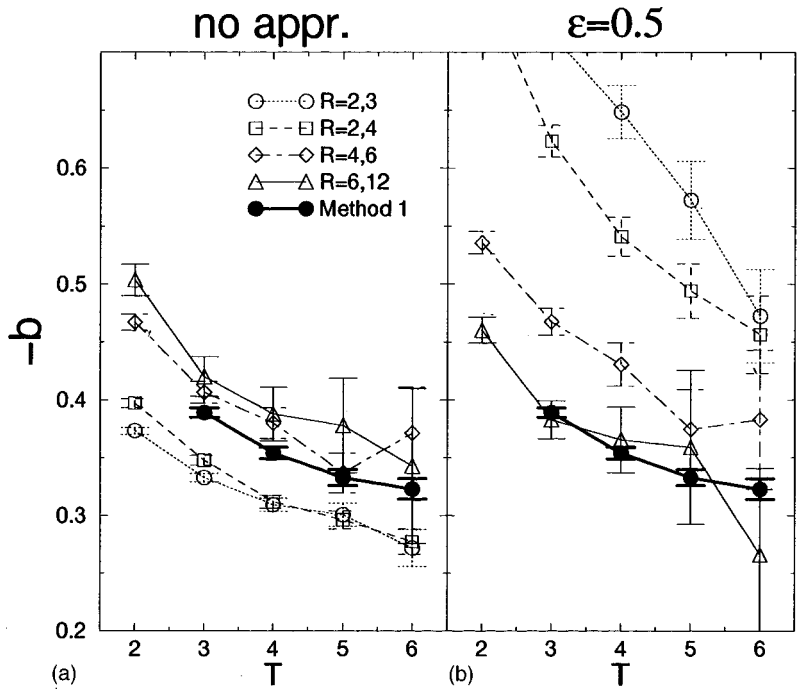

FIG. 14. Estimates of b at $\beta=2.5$ using (a) the continuum form of $V(R)$ [Eq. (4.6)] and, additionally, (b) a constant longitudinal profile approximation for the flux tube with $\epsilon=0.5$ [Eq. (4.9)].

Of more interest is the large-R limit, where it is expected from string models that both the action and energy flux tubes should have a form that is essentially constant for all R_L in the range $-R/2 \leqslant R_L \leqslant R/2$ with R-independent self-action or -energy terms concentrated at $R_L \approx \pm R/2$. As can be seen in Fig. 4, the sums over the transverse plane in the middle of the quarks agree at $\beta=2.4$ and 2.5, supporting the accuracy of our estimates in this region. Therefore, the action difference in Eq. (4.6), $\Delta\Sigma S=(\Sigma S_{R_1}-\Sigma S_{R_2})$, should be well approximated by $\Delta\Sigma S=[R_1 S_{R_1}(R_L=0)-R_2 S_{R_2}(R_L=0)]$ and similarly for $\Delta\Sigma E_L$ and $\Delta\Sigma E_T$ in Eqs. (4.7) and (4.8).

In practice, since $R_{1,2}$ are not very large, it is probably more realistic to include a correction for the ''overshoot'' of the plateau term at $R_L \approx \pm R/2$, i.e.,

$$\Delta\sum S \to \Delta\sum S' = [R_1(\mathrm{eff}) S_{R_1}(R_L=0) - R_2(\mathrm{eff}) S_{R_2}(R_L=0)], \qquad (4.9)$$

where $R_i(\mathrm{eff})=R_i+2\epsilon$. Here ϵ is the overshoot at each end of the plateau. From Figs. 4–6 it is seen that ϵ must be approximately one-half of a lattice spacing.

The results at $\beta=2.5$ with $\epsilon=0.5$ are shown in Fig. 14(b). The values of b approach those given by method 1 as $R_{1,2}$ increases, agreeing when $R_{1,2}=6,12$. The disagreement at the smaller R's is mainly due to significant self-energy contributions at the midpoint, which do not cancel as they vary with R. The good results from $R=6$ thus show that the self-energy contributions at the midpoint are negligible at these interquark separations. The same approximation can be used in the spatial sums of method 1. With $R=2,3$ excluded from the fit of Eq. (4.1) we get $b=-0.35(4)$ at $T=6$ and $\beta=2.5$.

The extracted value of b is only weakly dependent on ϵ even for the rather small values of $R_{1,2}$ used here. This situation will only improve as $R_{1,2}$ increases. In principle, this method has two advantages over the earlier ways of extracting b and f.

(i) It avoids the need for any delicate numerical cancellations of self-energies since they are assumed to have canceled exactly in the Δ's.

(ii) Only the single two-dimensional sum over the $R_L=0$ plane is necessary. This avoids the full three-dimensional sum of Eqs. (4.1)–(4.3). This estimate can be further improved by averaging the two-dimensional integrals over the smallest values of R_L. However, in practice this would not lead to savings in computer time since averaging over all positions and orientations of the Wilson loops would, in any case, mean using all possible planes in the lattice.

It has one disadvantage, however, in that it assumes a stringlike longitudinal dependence of the color flux distribution.

For large R one would expect that the string tension is given by the longitudinal energy density in the transverse plane at the midpoint:

$$b_S = 2\beta f E_L(R_L=0).$$

Taking the values of $E_L(R_L=0)$ from Fig. 4 and using our best estimates of f gives $\sqrt{b_S(2.4)}=483(15)$, $\sqrt{b_S(2.5)}=477(24)$ MeV. These are close to the values given by fits to experimental spectra.

D. Comparison with other approaches

There are two main ways to extract β functions in lattice gauge theories. First, one can measure observables at different values of some parameter (such as a coupling or a quark mass) and then try to estimate the response of the observable to a change in that parameter. This can be carried out using either finite differences or an interpolating function. Both of

TABLE V. Comparison between values of $b \equiv \partial\beta/\partial \ln a$.

β	Our estimate	Ref. [7]	Ref. [8]	Ref. [11]	Three-loop PT
2.4	$-0.312(15)$	-0.3018	$-0.305(6)$	$-0.330(4)$	-0.3893
2.5	$-0.323(9)$	-0.3115	$-0.312(2)$	$-0.340(4)$	-0.3889

these introduce a systematic error either from the use of a finite interval or from the choice of the interpolating function. In the second method, one can use the fact that response functions are related to correlation functions via lattice sum rules. This method has less systematic errors, but often leads to large statistical errors because the observables involve delicate cancellations.

In the case of SU(2) gauge theory, the first method has been used recently in Ref. [7], where b was estimated by measuring the critical temperature at six values of the coupling and using an exponential ansatz or a spline interpolation for the β dependence of a. In the same work, nonperturbative derivatives of couplings in the time and space directions with respect to the asymmetry factor $\xi = a_s/a_t$ were estimated from b and measurement of the free energy. In Ref. [11] lattice spacings were determined from the string tension at seven couplings in the range $2.3 \leqslant \beta \leqslant 2.85$ and fitted with an ansatz of a linear a dependence of $\Lambda_{\rm lat}$. The errors on these estimates do not include systematic effects from the use of a linear approximation. In Ref. [8] the lattice spacing was determined at six couplings ranging from $2.3 \leqslant \beta \leqslant 2.55$ through Sommer's equation $r_0^2 F(r_0) = c$ discussed after Eq. (2.1). Fitting of the three-loop relationship between a and β, with extra terms and systematic errors estimated using different values of c and forms of the fitted function lead to results consistent with Ref. [7].

The sum rule method was explored in Ref. [16], where $\partial V(R)/\partial\beta$ was fitted from the time dependence of Eq. (1.1) and b then extracted through a second fit of $\partial V(R)/\partial\beta$ vs R. Optimistically also potentials at $R=1$ were included in the fits. As this was only a feasibility study, the estimate of $b=-0.25(2)$ at $\beta=2.5$ should be considered as preliminary. A direct formula for b, Eq. (4.4), involving differences of two-body potentials at two values of R and their action sums was derived in Ref. [6]. An average over pairs of R values gave the estimate $b=-0.35(2)$ at $\beta=2.4$. The values at some R pairs were outside this estimate and doubts about the convergence in T remained, as the correlations were calculated only up to $T=4$ for larger R's.

Table V collects the most reliable estimates of b at $\beta=2.4$ and 2.5, whereas the available estimates of f are shown in Table VI. Here it should be noted that an effective coupling larger than the bare coupling moves the perturbative estimates of f closer to the nonperturbative values, whereas the opposite happens for b. A perturbative evaluation of b is thus unreliable. The nonperturbative estimates of b agree with each other, except for the one from Ref. [11], which has a significant systematic error. Averaging the three consistent estimates gives $b(2.4)=-0.306(6)$ and $b(2.5)=-0.316(4)$, which are 78% and 81%, respectively, of the three-loop predictions. For f our estimates are not far from those in Ref. [7], with ratios of the nonperturbative and perturbative estimates similar to those for b.

TABLE VI. Comparison between values of $f \equiv (U-S)/(2\beta)$.

β	Our estimate	Ref. [7]	PT
2.4	0.65(1)	0.72	0.85
2.5	0.68(1)	0.74	0.86

V. CONCLUSIONS

In this paper the spatial distribution and nature of the electric and magnetic color fields between two quarks are measured for $\beta=2.4$ and 2.5. We discuss carefully the theoretical expectations for scaling versus β of these distributions and compare with our results. For the observables with a well-controlled continuum limit (three-dimensional sums), scaling is investigated and found to be good in most cases of interest. For more differential observables (transverse sums and profiles) the changes seen between the two values of β can be explained qualitatively from the discretization: The plateaus stay the same, while the peaks get higher for smaller a. Self-energies, as measured by transverse plane sums, diverge in a manner suggested by leading-order perturbation theory, with the divergence being faster in the E_L case because of the longitudinal extent of the plaquettes measuring the dominant electric field. By comparing various combinations of the spatial sums of the $\mathcal{E},\mathcal{B}$ fields with the interquark potential $V(R) \pm \partial V(R)/\partial R$, estimates can be made of the generalized β functions b and f; see Eqs. (4.1)–(4.3).

There are two problems that prevent the direct use of these equations. First, since the whole calculation is performed on a lattice, $V(R)$ is only known at discrete values of R, so that the values of $\partial V(R)/\partial R$ cannot be measured directly. Second, both $V(R)$ and the spatial sums have self-action or -energy contributions. To minimize or avoid these problems the extraction of b and f can be carried out in different ways, each of which has its own advantages and disadvantages concerning statistical and systematic errors.

The most direct approach, method 1 of Sec. IV A, is to parametrize $V(R)$ so that $\partial V(R)/\partial R$ can be readily calculated. This overcomes the $\partial V(R)/\partial R$ problem at the expense of some systematic error introduced by the form of parametrization of $V(R)$ used. By plotting, as a function of R, $V(R) \pm \partial V(R)/\partial R$ versus the various spatial sums, the slopes give immediately b and f. This resulted in $b(2.4) = -0.312(15)$ and $b(2.5) = -0.323(9)$. However, the value of f was much more uncertain when the two sum rules, one involving ΣE_L and the other ΣE_T, were used separately. When these two sum rules were fitted simultaneously, a better result emerged, $f(2.4)=0.65(1)$ and $f(2.5)=0.68(1)$. Already at this stage, it could be seen that the data causing most of these uncertainties are those involving the longitudinal energy ΣE_L especially for $\beta=2.5$.

One way to avoid the $\partial V(R)/\partial R$ and self-action and -energy problems is to combine the original three sum rules in such a way as to eliminate the problems; see Eqs. (4.4) and (4.5) for method 2. However, in spite of the ideal form of these equations they result in poor estimates of both b and f. For $\beta=2.4$, b and f agree with method 1, but with large statistical errors; see Fig. 13(a). But for $\beta=2.5$ the values of b tend to be too low and of f too high, both with large error bars. These differences can be directly attributed to the inaccuracy of the data for ΣE_L.

The third method for extracting b and f exploits the form expected of $V(R)$ and the flux-tube profiles in the limit $R\rightarrow\infty$ from string models. When a continuum parametrization of $V(R)$ is used and two R values are subtracted, the sum rules reduce to those in Eqs. (4.6)–(4.8) and these yield results consistent with those of method 1, but with larger statistical errors. In the large-R limit, a further approximation is to replace the flux-tube profile by one that is constant between the quarks ($-R/2\leqslant R_L\leqslant R/2$) and dropping to zero rapidly for $R_L\geqslant R/2$ and $R_L\leqslant -R/2$. At the largest R's the results are consistent with method 1, but with large statistical errors. These results are only very weakly dependent on the point where the profile drops to zero beyond the positions of the quarks.

As seen in Tables V and VI, our best estimates for b and f agree with other recent nonperturbative estimates, most importantly the finite-temperature approach of Ref. [7]. It thus seems safe to conclude that order a^2 effects in the extraction of the β function are small at the β values studied using the methods described. Thus we have a unique nonperturbative β function that describes the deviations from asymptotic scaling at these values of the coupling.

For the state with A_{1g}' symmetry, our data show the existence of a dip in the action and transverse energy distributions away from the center of the flux tube in the transverse plane between the quarks. This qualitatively confirms the prediction of the Isgur-Paton flux-tube model for the energy distribution. No such node is seen for the longitudinal energy, and for the action it is more pronounced in the transverse component.

In the future we plan to study four-body flux distributions and their relationship to two-body flux tubes. Sum rules will be used verify the correctness of the measured distributions.

ACKNOWLEDGMENTS

The authors wish to thank P. Spencer for discussions during the initial stages of this work. Funding from the Finnish Academy (P.P.) is gratefully acknowledged. Most of the simulations were performed on the Cray C94 at the CSC in Helsinki.

[1] A. M. Green, C. Michael, and P. S. Spencer, Phys. Rev. D **55**, 1216 (1997).
[2] C. Michael, Nucl. Phys. **B280**, 13 (1987).
[3] H. J. Rothe, Phys. Lett. B **355**, 260 (1995).
[4] H. J. Rothe, Phys. Lett. B **364**, 227 (1995).
[5] C. Michael, Phys. Rev. D **53**, 4102 (1996).
[6] C. Michael, A. M. Green, and P. S. Spencer, Phys. Lett. B **386**, 269 (1996).
[7] J. Engels, F. Karsch, and K. Redlich, Nucl. Phys. **B435**, 295 (1995).
[8] P. Pennanen, Phys. Rev. D **55**, 3958 (1997).
[9] R. Sommer, Nucl. Phys. **B411**, 839 (1994).
[10] R. Sommer, Nucl. Phys. **B306**, 181 (1988).
[11] G. S. Bali, K. Schilling, and C. Schlichter, Phys. Rev. D **51**, 5165 (1995).
[12] M. Baker, J. S. Ball, and F. Zachariasen, Phys. Rev. D **51**, 1968 (1995).
[13] M. Baker, J. S. Ball, and F. Zachariasen, Int. J. Mod. Phys. A **11**, 343 (1996).
[14] N. Isgur and J. Paton, Phys. Rev. D **31**, 2910 (1985).
[15] F. Karsch, Nucl. Phys. **B205**, 285 (1982).
[16] G. S. Bali, C. Schlichter, and K. Schilling, Phys. Lett. B **363**, 196 (1995).